Journal of Alloys and Compounds 735 (2018) 2574–2583

Contents lists available at ScienceDirect

Journal of Alloys and Compounds

journal homepage: http://www.elsevier.com/locate/jalcom

Temperature-induced transformations and martensitic reorientation processes in ultra-fine-grained Ni rich pseudoelastic NiTi wires studied by electrical resistance

J.L. Pelegrina [a, *], J. Olbricht [b, 1], A. Yawny [a], G. Eggeler [b]

[a] Centro Atómico Bariloche, Instituto Balseiro and CONICET, 8400 San Carlos de Bariloche, Argentina
[b] Institute for Materials, Ruhr University Bochum, 44780 Bochum, Germany

ARTICLE INFO

Article history:
Received 22 August 2017
Accepted 2 December 2017
Available online 5 December 2017

Keywords:
Shape memory alloys
NiTi
Martensitic transformation
Electrical resistance

ABSTRACT

Temperature-induced, stress-induced martensitic phase transitions and martensite reorientation process in Ni rich (50.9 at.%) NiTi pseudoelastic NiTi wires with ultra-fine grained (UFG) microstructure were studied by electrical resistance measurements. Measurements of the electrical resistance as a function of temperature at different constant mechanical loads accompanied by complementary experiments with variable loads at constant temperature were performed. Results show that the transformation mechanisms in UFG microstructures exhibit a higher level of complexity when compared with those characterizing the behavior of other microstructures (e.g., recrystallized or larger grains size). It was found that a threshold stress level below 150 MPa delimits the transition from a homogeneous (low stress) to localized but reversible Lüders type transformation (high stress) when the transformations are induced under constant applied stress and that reorientation processes require stresses of 100 MPa in the present UFG wires. Even though the strain evolutions do not always show two distinct yielding events during cooling or heating, electrical resistance measurements proved that a two-step transformation involving R-phase and B19′ martensite was always present in the extended range of temperatures and stresses investigated here.

1. Introduction

NiTi alloys with near-stoichiometric composition are widely used shape-memory materials because they combine good mechanical and functional properties [1,2]. The special characteristics, such as shape memory and pseudoelasticity, rely on diffusionless martensitic transformations which characterize these materials. In the case of NiTi shape memory alloys up to three phases are involved. The high temperature phase, often referred to as the parent phase, is characterized by an ordered cubic structure of type CsCl (Strukturbericht symbol: B2) [3]. The low temperature phase, called martensite, has a monoclinic structure (B19′) [4]. Between B19′ and the B2 phase twelve lattice correspondences exist. Therefore, martensite variants which are twin-related can form in each B2 grain, allowing for self-accommodation and minimization of the overall strain energy [3]. Depending on the composition of the alloy and the imposed thermomechanical treatment, a third martensitic phase may appear in an intermediate temperature range. This phase is called the R-phase. It exhibits a characteristic rhombohedral structure [5] and also presents a variant morphology with respect to the B2 phase. During the transformation either from the parent phase or the R-phase to the low temperature phase, twinning events constitute lattice invariant shear processes which occur in each B19′ region [3].

At present, most NiTi applications rely on material that is subjected to a thermomechanical treatment. This treatment induces an ultra-fine grained (UFG) microstructure that keeps dislocation plasticity at a minimum and therefore results in improved functional properties [6]. In recent years, extensive research has been carried out to rationalize this behavior [7–9]. UFG NiTi typically exhibits a two-step martensitic transformation involving all three phases introduced above. Fig. 1 illustrates this transformation behavior for a commercial Ni-rich (50.9 at.% Ni) UFG NiTi wire [10], identical to the one which will be further characterized in the

* Corresponding author.
E-mail address: jlp201@cab.cnea.gov.ar (J.L. Pelegrina).
[1] Now with: BAM Federal Institute for Materials Research and Testing, 12200 Berlin, Germany.

https://doi.org/10.1016/j.jallcom.2017.12.009
0925-8388/

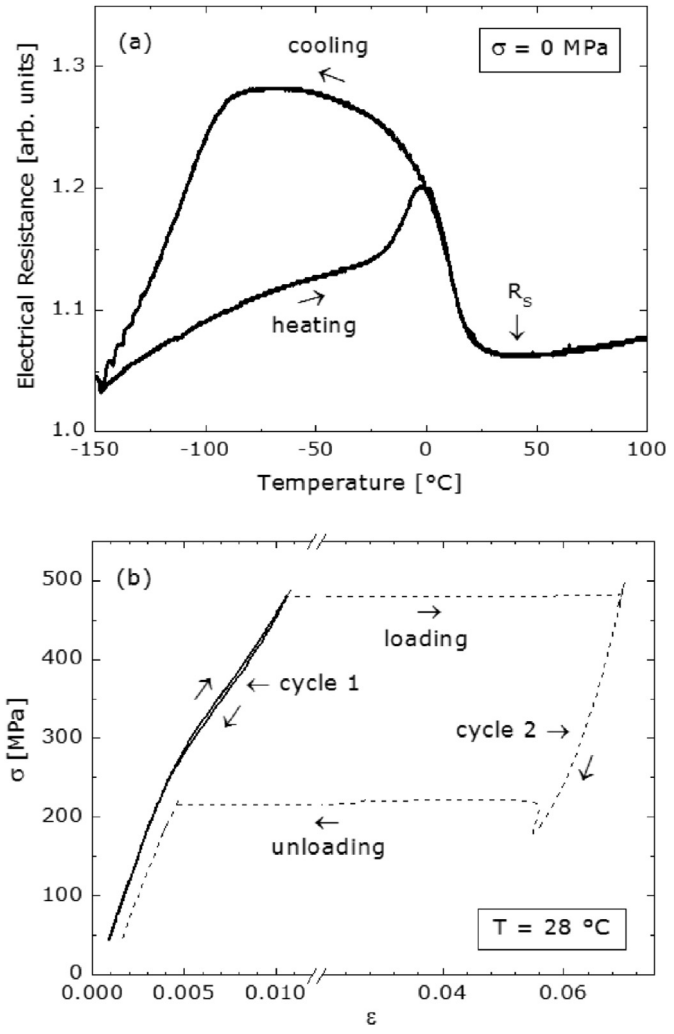

Fig. 1. Evidence of the martensitic phase transformation in a NiTi wire specimen. (a) Variation of electrical resistance during a cooling/heating cycle (load-free condition), (b) stress-strain behavior during loading at a constant temperature.

present work. In Fig. 1a, the temperature dependence of the electrical resistance in arbitrary units (*E.R.-T*) is presented. It can be appreciated how the transformation sequence affects the electrical resistance of a specimen subjected to a cooling/heating cycle for the case in which the wire is free of external mechanical load. Starting from the B2 phase, the microstructure of the material will progressively change, passing through stages where B2, different R-phase and B19′ variants might coexist in different proportions as proposed in Ref. [10]. Detailed investigations of such microstructures have shown that these variants are organized in a self-accommodating arrangement which minimizes the macroscopic shape change of the specimen [3,11,12]. Literature data suggests that when compared at the same temperature, the electrical resistance of the B2 phase is lower than that of B19′ martensite, which in turn is lower than that of the R-phase [13,14]. On cooling from 100 °C, the initial linear decrease of resistance of the B2 phase (normal metallic behavior) changes at around 30 °C. Here, the formation of R-phase results in an increase of the electrical resistance with decreasing temperature. To characterize this gradual change of electrical resistance, a temperature delimiting both regimes can be identified. It can be interpreted as the onset of the R-phase formation on cooling and is referred to as R_S in Fig. 1a. On further cooling, B19′ martensite eventually starts to form but, as will be shown later, it is not trivial to identify a distinct starting point. The ongoing transformation results in a decrease of the *E.R.-T* curve at temperatures below −100 °C which continues down to a temperature of −150 °C where cooling was stopped [10]. Upon heating from this temperature, a moderately non-linear *E.R.-T* response is observed in the temperature range between −150 °C and −25 °C. Then, around 0 °C, a distinct peak associated with the reverse transformation to the parent phase appears which extends up to around 25 °C. Thereafter, the linear *E.R.-T* metallic behavior of the B2 phase is again observed on further heating. As general characteristic, it can be seen that the heating part of the *E.R.-T* cycle intersects the cooling part of the curve in the region associated with the R-phase formation. The whole cycle can be divided then in two sub cycles, one at lower temperatures where cooling/heating paths are anti-clockwise and one at higher temperatures and mainly associated with the R-phase where the cooling/heating path is clockwise.

The martensitic transformations may also be mechanically induced. Fig. 1b illustrates this second transformation scenario for the case where a similar UFG NiTi wire was deformed to a strain of 7% at a constant temperature of 28 °C. First, the stress increases almost linearly up to about 250 MPa and that can be interpreted as the elastic deformation of the B2 austenite phase. In the stress range from 250 MPa to 475 MPa a deviation from linearity is observed than can be attributed to the stress induced transformation to R-phase. In this stage, the accumulated total strain reaches a value of approximately 1% and includes the contribution associated with the phase transformation from B2 to R-phase and also the elastic contributions of both coexisting phases [15]. This total deformation is reversible as can be appreciated in the complete loading/unloading cycle denoted as cycle 1 in Fig. 1b. On further straining, the material continues deforming at constant stress in the strain range from 1% to 7%. This deformation is associated with the transformation to B19′ martensite [16]. On reverting the imposed strain, the reverse transformation from B19′ occurs at a stress level around 220 MPa below the plateau level for the forward transformation. This gives rise to a hysteresis loop for the complete cycle (cycle 2 in Fig. 1b). Both plateau-like horizontal sections of the stress-strain curve in Fig. 1b are associated with the propagation of transformation fronts, leading to a highly-localized mode of transformation (Lüders bands) [7,17,18]. Note that the specimen nearly recovers its original length after reaching a deformation of up to 7%. The mechanical behavior just described is referred to as pseudoelasticity. As in this case the B19′ martensite forms under an applied mechanical stress, it is expected that the induced martensite variants are those which are more favorably oriented with respect to the applied stress. It is important to remark here that the stress induced formation of R-phase described before does not show the typical Lüders band features accompanying the stress induced formation of the B19′ martensite; on the contrary, as it was shown in Refs. [10,19], the R-phase forms homogeneously along the length of the specimen.

A third transformation scenario can be found if the martensitic transformation is induced by lowering the temperature, but in the presence of an applied constant load. In this case, it is expected that the distribution of variant orientations depends on the applied load, adopting intermediate configurations between those corresponding to the two previously described scenarios according to the actual stress level. The loading situation closely resembles the typical operational conditions of shape memory materials in different actuator applications like, e.g., gripping or positioning devices [20]. The experimental characterization of these more complex transformation processes in UFG microstructures, characteristics of commercial pseudoelastic NiTi wires, has so far received little attention despite their technological relevance

[10,21]. For example, only recently, the effect of temperature on the reorientation of load-free thermally induced martensite variants has been addressed by Laplanche et al. in Ref. [22], but considering recrystallized NiTi wires and ribbons.

Due to the its relative importance, the focus of the present work is set on providing a comprehensive analysis of the transformation characteristics of UFG NiTi wires in thermal cycles under mechanical load, considering also martensite variants reorientation processes taking place at low temperatures. Since, as was shown above, the different phases in NiTi shape memory alloys exhibit substantially different electrical resistivity values, electrical resistance measurements are employed here as the central tool for assessing the transformation activity. Dedicated complementary experiments clarify the impact of different basic deformation processes (elastic deformation, the martensitic transformations, variant reorientation in the martensitic phases, and the generation of microstructural defects) on the electrical resistivity response to demonstrate its applicability in the analysis of shape memory phenomena.

2. Experimental procedures

Ti-50.9 at.% Ni commercial wire with a diameter of 1.2 mm (Memory Metalle, Weil am Rhein, Germany) was investigated in the present study. During manufacturing, the material was hot worked, subjected to various steps of wire drawing and intermediate annealing, with a final annealing under load at about 793 K (520 °C) for 60 s followed by a chemical cleaning step to remove surface oxides. The combination of strong cold work followed by a short annealing results in an UFG microstructure. Additional information on the material used in the present study was reported elsewhere [10,23].

A first set of mechanical experiments was carried out in a Gabo Eplexor testing device (max. force capacity 500 N) which was equipped with an environmental chamber for operation between −150 °C and +500 °C. Wire specimens of 50 mm length, including a gauge length of 30 mm and twice 10 mm for gripping, were used. A fresh specimen was used for each experiment. All stress values given in the present work were calculated based on the wire diameter in the as-received condition, i.e., 1.2 mm. The specimens were first heated up to +100 °C to assure a fully austenitic condition prior to further testing, Fig. 1a. Thermal cycling was performed under different levels of constant load. The imposed cooling and heating rates were 0.033 °C/s (2 °C/min). In some cases, the cooling/heating was interrupted and a loading/unloading cycle was performed at constant temperature. In these experiments, mechanical loading and unloading was performed in displacement control at a speed of 0.2 mm/min. The evolution of electrical resistance of the specimens was determined using an alternating current potential drop (ACPD) system ACMS-M (Matelect Systems Inc., Canada). The four leads method was applied, employing NiCr wires as current and potential leads. The current leads were screwed to the grips and those for potential drop measurement were spot welded to the specimen in the 15 mm central section of the gauge length. An electrical current with a frequency of 500 Hz and a constant RMS intensity of 100 mA was applied. This frequency is low enough to reduce the significance of the skin effect, thus ensuring a nearly uniform current density in the specimen cross section [24].

Additional experiments were performed in a servohydraulic testing machine MTS 858 Mini Bionix II with the objective of correlating the *E.R.-T* behavior with the corresponding strain vs. temperature (ε-*T*) response. The experimental procedure was similar as before, except that the minimum accessible testing temperature was limited to 213 K (−60 °C) and the gage length was 35 mm. In these experiments, the electrical potential drop was also monitored in a 15 mm probe region contained in specimen's gauge length.

To avoid undesired local stress concentrations that could alter the transformation behavior of the specimens, the use of contacting extensometers was avoided in the experiments. Thus, all strain values reported in the present study were calculated from displacement signals of the respective testing machines.

3. Results and discussion

To illustrate on the consequences of an applied load on the electrical resistance response during thermal cycles, *E.R.-T* curves for two selected loads, 50 MPa (Fig. 2a) and 150 MPa (Fig. 2b) are presented in Fig. 2. The curve for the load-free case of Fig. 1a was added to both diagrams for direct comparison (dotted lines in Fig. 2a and b). All *E.R.* data were normalized using the corresponding values at 348 K (75 °C), temperature level corresponding to stable austenite.

Three significant changes can be observed when comparing these two mechanically loaded conditions with the load-free situation. First, there is a shift of the maxima on cooling (marked with

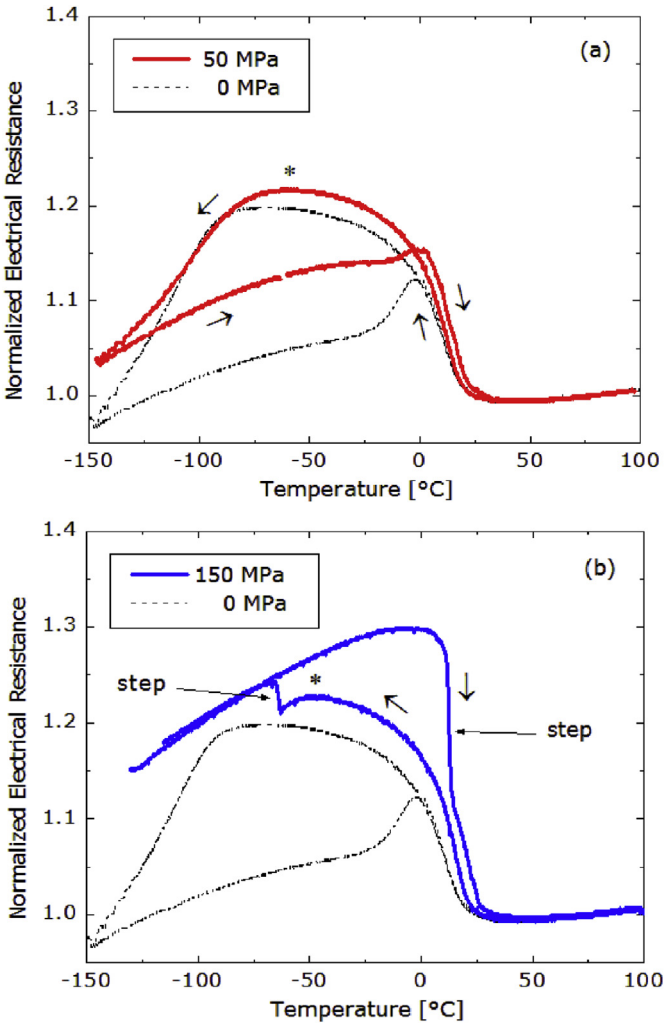

Fig. 2. Variation of the electrical resistance in temperature cycles under constant loads of (a) 50 MPa and (b) 150 MPa. Arrows identify the cooling/heating branches of the curves under load. The data set of the load-free case (cf. Fig. 1a) was added to both diagrams for comparison. See text for details.

asterisks in Fig. 2) towards higher temperatures and towards slightly higher normalized electrical resistance. The second peculiarity is apparent in Fig. 2b where for the stress of 150 MPa, sudden resistance changes (steps) appear during cooling and heating. These abrupt variations were shown to be related to the localized transformation to martensite [21] as will be discussed later. A third difference is associated with the shapes of the *E.R.-T* curves. At 50 MPa, the general shape of the *E.R.-T* cycle is similar to the one corresponding to the load-free case (0 MPa) described in the Introduction section. In contrast, at 150 MPa, for a same temperature, the resistance during heating is always higher than that observed during the previous cooling stage with the full cycle now exhibiting a clockwise appearance.

To allow for a more detailed analysis, the respective cooling and heating branches of various tests performed at different constant stresses up to 300 MPa are plotted separately in Fig. 3a and b, respectively. For loads of 50 MPa (curve 2) and 100 MPa (curve 3), the *E.R.* peak on cooling is shifted towards higher temperatures and higher normalized resistance values. After passing the respective maxima, a more pronounced change in slope develops. This is followed by a region of almost linear *E.R.* behavior whose extension increases with increasing load. At a stress of 150 MPa (curve 4), a resistance step is for the first time detected. In this case, it occurs approximately 25 K after the peak maximum. At an applied stress of 200 MPa (curve 5), a similar resistance step appears at a higher temperature compared with the 150 MPa case. It takes place shortly after the maximum is reached and its magnitude becomes more prominent. These trends continue at the 300 MPa case (dark yellow), leading to a pronounced step which now occurs before a maximum in the electrical resistance curve is detected.

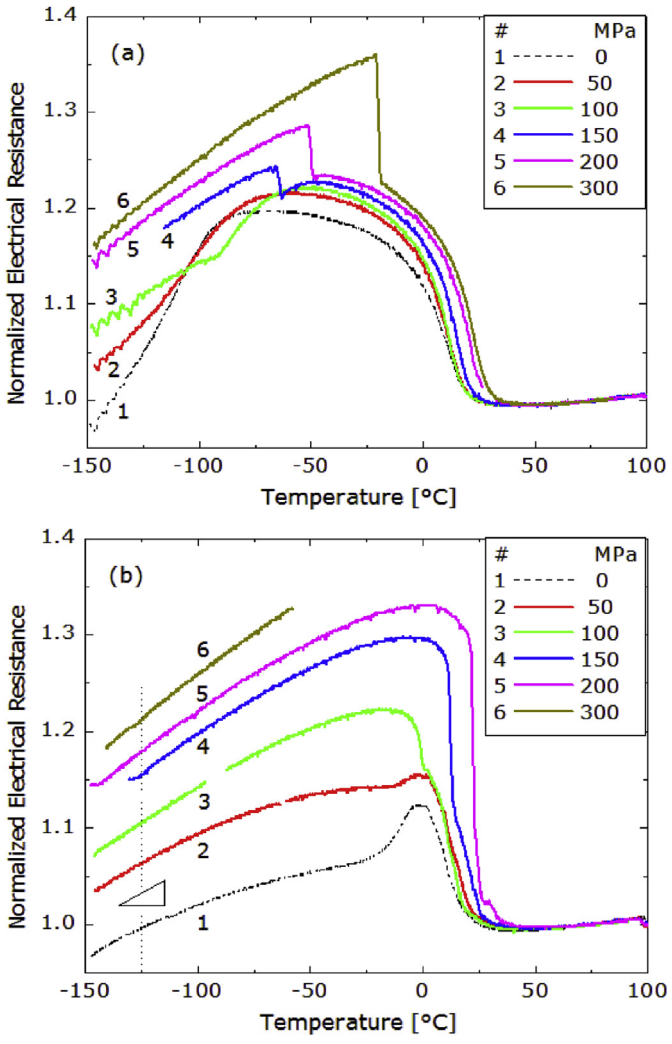

Fig. 3. Variation of the electrical resistance in temperature cycles under different constant loads on (a) cooling and (b) heating. See text for further details.

When analyzing the behavior during heating (Fig. 3b), it can be seen that the position of the resistance peak in the 50 MPa case does not change significantly compared with the load-free situation, but its relative intensity with respect to the low temperature side *E.R.* values decreases. At stresses above 100 MPa, a step like drop in electrical resistance begins to manifest. The resistance steps are well defined with the magnitude of the associated resistance change increasing both on cooling and heating (heating data of the 300 MPa test in Fig. 3b is incomplete due to systematic specimen slippage). For each stress level, the resistance change associated with the steps is higher on heating than on cooling although the temperature intervals of the steps are nearly similar in all cases with values between 1 K and 2 K.

Fig. 3b also shows that the maxima in the *E.R.-T* curves develop in two different ways. In the case of 50 MPa, the peak maximum is reached after two times changing the curvature sign, similarly to what occurs in the case where no load is applied. Instead, at higher stresses, no changes in the sign of curvature are observed before the *E.R.* maxima are reached. The development of these maxima is strongly related with the subsequent appearance of the step down in electrical resistance. The gradual non-linear variation of *E.R.* in a temperature range around the maximum indicates the occurrence of homogeneous transformation activity before the step-like localized transformation takes place. The temperatures associated with the step positions increase with the applied stress, Fig. 3b. After the step, further transformation activity is still observed in a limited temperature range in all the cases.

To better identify the underlying deformation mechanisms responsible of the observed behavior, it would be convenient to consider the shape change of the specimens in the different phases of the cooling/heating cycles. In Fig. 4, results of experiments performed in the servohydraulic testing machine, which allowed the simultaneous measurements of electrical resistance and mechanical deformation, are presented to analyze possible correspondences between the *E.R.-T* behavior and the ε-*T* response. The data correspond to the case of a transformations induced by cooling under constant applied stresses of 40 MPa (Fig. 4a) and 300 MPa (Fig. 4b). In both cases, the black curve represents the strain evolution with temperature after subtracting the thermal contraction contribution of the B2 phase from the original data while the colored curve shows the variation of *E.R.* of the 15 mm probe region on the specimen after subtracting the temperature dependence of the *E.R* of the B2 phase from the original data. The comparison between the *E.R.-T* curves for similar applied stresses has been made on occasion of discussing Fig. 3; here the attention will be focused more on the ε-*T* response.

The ε-*T* curve corresponding to 40 MPa (Fig. 4a) indicates only a marginal variation of the strain in the whole explored temperature range. In the intermediate region where both *E.R.-T* curves show a similar continuous development, the evolution of the respective ε-*T* curves is significantly different, i.e., the total strain variation in the case of 40 MPa is close to 0.5% while a strain variation of around 2% is reached at the point where a sudden and considerable strain step appears in the 300 MPa case. This step like variation is located at the same temperature level of −25 °C where a corresponding *E.R.* step occurs. An elongation of the specimen by about 5% is identified. This value is close to typical transformation strains associated with the stress induced formation of B19' (6%–7%) reported in the

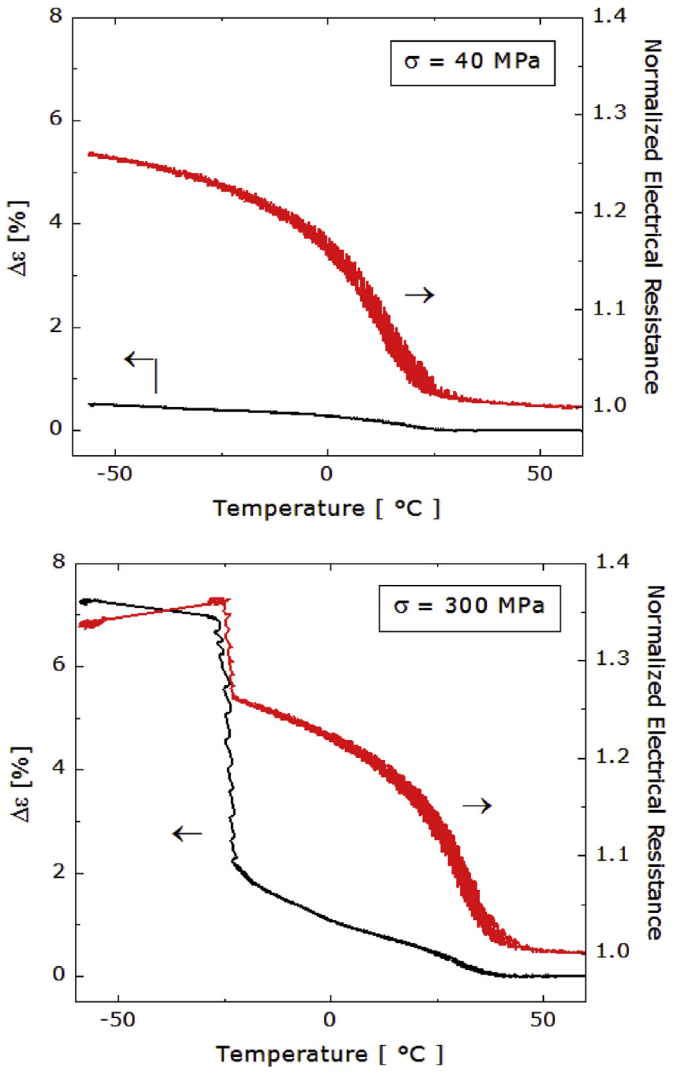

Fig. 4. Evolution of strain and electrical resistance on cooling under an applied stress of (a) 40 MPa and (b) 300 MPa. See text for details.

literature [16] and clearly exceeds the maximum strains reported for R-phase formation (~1%) [15].

In a previous work [21], it was shown that steps observed in the *E.R.-T* curves corresponded to the propagation of one or few transformation fronts during a so-called localized transformation to B19′ martensite. In this way, the specimen locally changes from a mainly austenitic to a mainly martensitic state when the transformation front passes by, leading to a sudden alteration of the local resistive properties of the material. This temperature-induced localized transformation is analogous to the localized transformation behavior observed during pseudoelastic loading and represented in Fig. 1b [7,17,18]. In that case however, the amount of transformed material per unit time is controlled by the imposed displacement rate which limits the shape change. In the present experiments, the temperature is varied and the elongation of the test piece is not limited, leading to more abrupt responses. Such abrupt responses would also be observed in a pseudoelastic cycle like the one represented in Fig. 1b when, instead of imposing the displacement on the specimen, the experiment would be conducted under load control. This subtle difference results from the equivalent thermodynamic role of stress and temperature in these first order phase transformations. It may therefore be concluded that the resistance and strain step upon cooling shown Fig. 4b result from a localized transformation to B19′ martensite.

The similarities between the shape of the *E.R.-T* curve for the 40 MPa with the one corresponding to 300 MPa before the step, suggest also that similar transformation processes are occurring in the respective temperature intervals. The smooth and continuous change indicates that the underlying transformation processes here takes place in a homogeneous manner throughout the specimen gage length, with the volume fraction of the induced martensitic phases continuously increasing as the temperature is decreased. However, in the case of 300 MPa, more variants with preferred orientations are formed which results in a certain elongation of the specimen. Taking into account the above described characteristics and previous results published in the literature on the same material [10], we conclude here that both thermally induced R-phase and B19′ martensite with a certain degree of preferred orientation is homogeneously formed along the length of the specimen in the region where gradual developments of the *E.R.-T* and ε-*T* curves are observed. The degree of preferred orientation increases the higher the applied stress is. The formation of oriented B19′ is proposed considering that the maximum strain associated with the well oriented R-phase formation is around 1% [10] and here values close to 2% are reached. The just described homogeneous transformation behavior is interrupted by the localized formation of B19′ martensite when the stress level is high enough and the step like behavior is observed. In effect, considering that the occurrence of a step-like change of resistance implies a localized transformation mechanism, the material response shown in Fig. 3a indicates the existence of a stress threshold level demarking the occurrence of a localized mode of transformation to B19′. For the material investigated here, this threshold level falls into a stress region below 150 MPa. For stresses below this value, the formation of B19′ martensite is therefore non-localized. Above the threshold level, heterogeneous transformation to B19′ occurs and its dominance increases with the applied stress (Fig. 3a). The coincidence between the steps observed in electrical resistance and strain curves in Fig. 4b indicates that these newly formed B19′ variants are favorably oriented with respect to the applied stress, resulting in higher strain values.

It is important to mention here that, even though electrical resistance and mechanical data included in Fig. 4b show qualitatively similar characteristics, the step-like B19′ formation is dominant in terms of the associated relative strain increment compared to the preceding R-phase, whereas its impact on the relative *E.R.* variation remains quite limited compared to the R-phase transformation step. This suggests that electrical resistance is more sensitive in detecting the presence of the homogeneous transformation while strain information reacts better to the heterogeneous transition.

Further insight into the individual contributions of the different transformation and reorientation processes could be gained by analyzing, at certain specific temperatures, the variation of *E.R.* with the stress level associated with the curves represented in Fig. 3a and b. Two temperature levels were considered here. First, a temperature of −47 °C on cooling, which is close to the value where local maxima occur in Fig. 3a and where a mixture of the three phases (i.e., B2, R-phase and B19′) is expected. Second, a temperature of −125 °C on heating, after previously having reached −150 °C on cooling. In this latter case, B19′ martensite should be the dominant phase for all considered stress levels since no discernible retransformation event is detected in the *E.R.-T* curves on heating from −150 °C to −125 °C. In Fig. 5, the normalized *E.R.* values obtained from the experiments shown in Fig. 3 are plotted as a function of the applied stress. The data sets show that in both cases the *E.R.* values increase with mechanical stress when compared

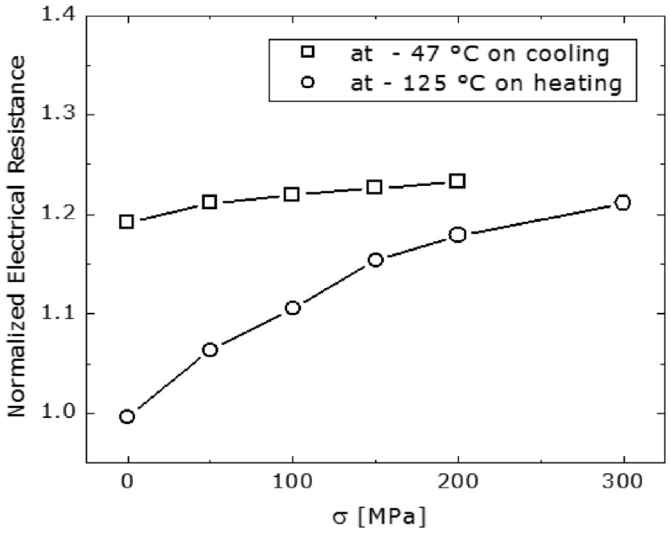

Fig. 5. Electrical resistance vs. applied stress for two particular temperatures.

with the load-free case. The increments are about 3% at −47 °C for a maximum stress of 200 MPa and 22% at −125 °C for a maximum stress of 300 MPa.

The increase in *E.R.* with the applied load shown in Fig. 5 might be consequence of different, simultaneously acting processes, besides the changes in the volume fraction of phases, variant reorientation processes and the creation of internal interfaces. They include the geometrical variations associated with the elastic deformation of the specimen and also defects that might be introduced as a consequence of plastic deformation due to the high acting mechanical stresses. In particular, the electrical resistance (*E.R.*) of a NiTi wire specimen is a function of its length l and radius r, the resistivity $\rho_i(T)$ of the individual phases, microstructural parameters m_k ($k = 1, 2, ..., n$) representing the phase volume fraction, their orientation distribution, the density of interfaces, etc. and additional microstructural parameters m_d describing density and distribution of defects (e.g., dislocations, grain boundaries, etc., with $d = 1, 2, ..., m$), the temperature T and the thermal expansion coefficient α. These dependencies can be expressed in general terms by the following equation:

$$E.R. = f\,[\,\rho_i(T)\,;\; l(T,\alpha,\varepsilon)\,;\; r(T,\alpha,\varepsilon)\,;\; m_k\,(T)\,;\; m_d(T)\,] \qquad (1)$$

An evaluation of the relative importance of the above mentioned factors on the electrical resistance is firstly performed in what follows.

The contribution of the elastic deformation is analyzed first. For the analysis of the data presented in Fig. 5, the effect of the elastic strain can be in a first approximation attributed solely to changes in the geometry of the specimen (length l and radius r). Assuming a mean value of the Poisson ratio ν for the material with a complex microstructure, the variation of the electrical resistance with the elastic strain at constant microstructure can be estimated from:

$$E.R.(\varepsilon) = E.R.(\varepsilon = 0)\frac{(1+\varepsilon)}{(1-\nu\,\varepsilon)^2} \qquad (2)$$

By considering a typical value of $\nu = 0.33$ and a maximum strain value for the elastic range of 1 E-3, it turns out that the maximum influence on electrical resistance is limited to about 0.2% (0.002), whichever phases are present. *E.R.* variations of this magnitude are negligible when compared with the total changes in electrical resistivity observed in Figs. 2, 3 and 5.

Next, the possible contribution of defects (parameter m_d) that might be introduced in the different phases involved due to the high stress levels being present during the martensitic transformation is evaluated as follows. In Fig. 6a, the stress-strain behavior obtained in a wire specimen upon repeated mechanical loading/unloading at constant temperature is presented. The first three cycles of transformation are shown and only the stress-strain curves obtained on loading are plotted for the sake of clarity. In all cycles, the initial almost linear loading range is followed by a transformation plateau. The stress level characterizing this plateau like part of the loading curves decreases with each new cycle. This effect is usually referred to as functional fatigue [25] and is rationalized based on defects being introduced during the transformation [26]. The inset in Fig. 6a schematically illustrates the distribution of phases in the specimen when the stress reaches the constant transformation plateau value and the deformation is still small taking into account that the martensitic transformation occurs in a localized mode. Consequently, martensite (black parts of the specimen) has nucleated in the gripping area due to local stress concentrations, but the advancing transformation fronts have not yet reached the region where the resistance of the specimen is measured by the electrical probe. A previous study [10] on identical material was able to show that the microstructure in the probe

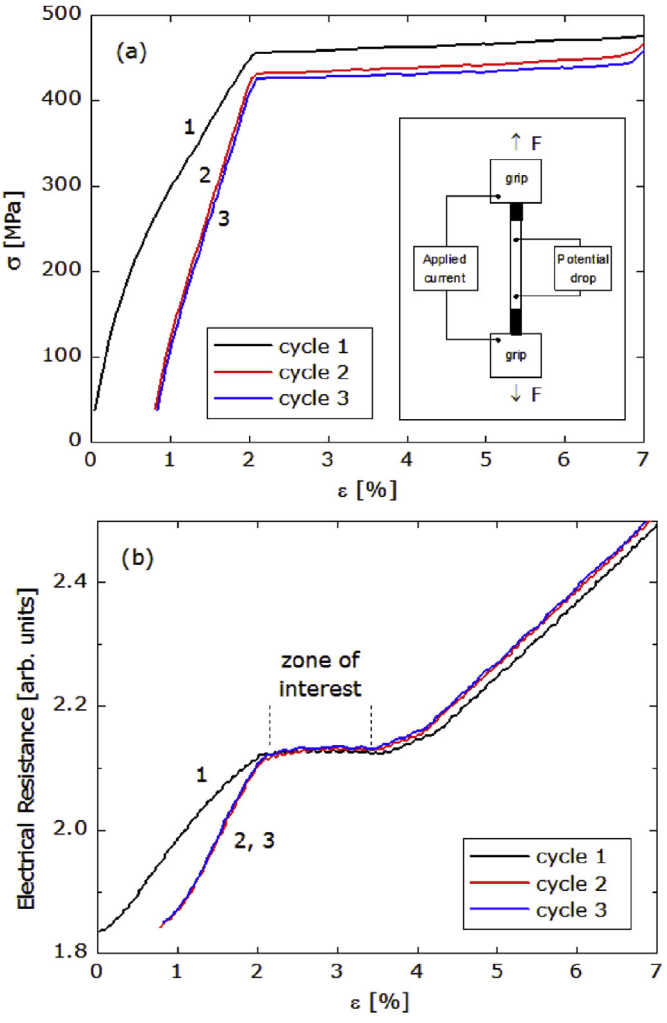

Fig. 6. Three consecutive stress-induced transformation cycles (only the loading part is shown). (a) Stress vs. strain and a schematic view of the state of the sample at the initial stages of the transformation plateau, (b) Evolution of the electrical resistance during these load cycles as a function of strain.

region then consists of a mixture of parent and R-phases. It was also shown in Refs. [10,27,28] that the UFG microstructure is sufficiently strengthened by its thermomechanical treatment to avoid early defect introduction in the austenitic (B2) or R-phase condition. Non-recoverable strains and a decay of functional properties were only detected in specimen regions that had undergone the transformation to B19′ martensite. Returning to Fig. 6, the previous considerations indicate that only when the transformation fronts enter the probe region, defects will be introduced in that zone and they will increase their density with further cycling. However, for each individual cycle, in the interval between the onset of the transformation plateau and the entrance of the transformation front into the probed region, a constant value of electrical resistance is expected because the load as well as the local phase composition remains constant. In the *E.R.*-ε plot shown in Fig. 6b, corresponding segments are observed for all three cycles in the 2% to 3.5% strain region. It is interesting to note that, despite the obvious decrease of transformation plateau stresses displayed in Fig. 6a, the resistance value does not vary with the number of mechanical cycles. This finding suggests that the effect of the increasing defect density on *E.R.* is negligible and cannot therefore explain the observed stress-dependence of the electrical resistance in thermally-induced transformations under load.

The previous analysis allow to discard the contributions of the elastic deformation and of the defects introduced by cycling on the *E.R.* evolutions. The similarity of the slopes of the *E.R.-T* curves at −125 °C (vertical dashed line in Fig. 3b) suggests that a constant and equal amount of phases is present, independent of the applied stress. Therefore, the about 22% variation of *E.R.* detected doing thermal cycles under constant load (circles in Fig. 5) can be interpreted as a result of martensitic variants reorientation processes.

To gain further understanding on the effect of the reorientation of variants and the change in the proportion of phases when loading at low temperatures will now be analyzed. For this purpose, additional experiments were performed in which three similar specimens were firstly cooled down to −100 °C, −125 °C and −150 °C, respectively, then deformed until the same maximum applied stress, then unloaded keeping the temperature constant and finally heated up to austenite. The whole procedure resembles the typical temperature-stress-strain path used to characterize the one-way shape memory effect and specific details will be given next. These experiments were performed in the Gabo Eplexor testing setup and during cooling, a small constant preload equivalent to a stress of 6 MPa was applied for practical reasons to avoid loosening of the load chain. The evolutions of electrical resistance during cooling are shown in Fig. 7a where numbers 1, 2 and 3 indicate the *E.R.-T* points corresponding to the minimum temperature reached in each case. Fig. 7a includes as a reference the *E.R.-T* curve for cooling under an applied constant stress of 300 MPa and also some additional information that will be considered later. The *E.R.-T* evolutions on cooling fall on a common curve, i.e., the one representing the behavior shown in Fig. 1a for the load-free condition. Depending on the minimum reached temperature, a different proportion of phases is present before increasing the load up to 300 MPa, after waiting 120 s to attain thermal equilibrium. The evolution of *E.R.* with strain at constant temperature during the respective loading processes is shown in Fig. 7b while the

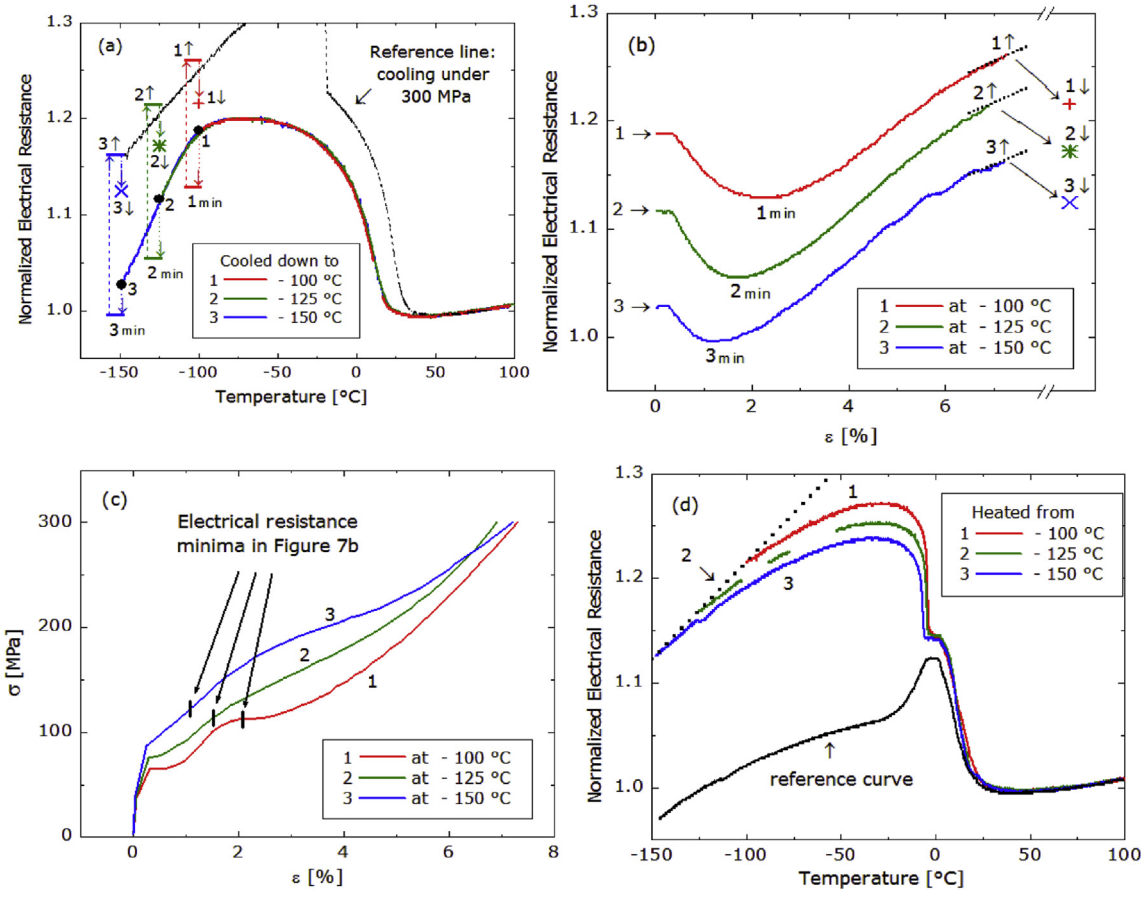

Fig. 7. Mechanical loading experiments at low constant temperatures. (a) Electrical resistance vs. temperature on cooling at an applied load of 7 N (before the loading experiment). (b) Evolution of electrical resistance with strain at low temperature. (c) Stress-strain behavior associated with the evolution in (b). (d) Electrical resistance vs. temperature on heating (after the loading/unloading sequence).

corresponding stress vs. strain curves are shown in Fig. 7c. All curves shown in Fig. 7b exhibit a similar behavior with an initial short strain range where resistance values remain constant followed by a decrease to a minimum and finally by a monotonous increase until the stress of 300 MPa is reached. The respective minima are denoted by 1_{min}, 2_{min} and 3_{min} in Fig. 7b while the points corresponding to the stress of 300 MPa by $1^{\uparrow}$, $2^{\uparrow}$, $3^{\uparrow}$. The *E.R.* values after unloading are those corresponding to the points denoted as $1_{\downarrow}$, $2_{\downarrow}$ and $3_{\downarrow}$ and included at the right of Fig. 7b. These three set of characteristic data points are also represented in Fig. 7a to facilitate further analysis.

It can be seen from Fig. 7b that the minima in *E.R.* occur at lower strain and lower *E.R.* values the lower the loading temperature is. Concerning the high strain part of the curves, it is possible to confirm that at the 300 MPa stress level, the transformation and/or reorientation processes are completed. For this purpose, the variation of resistance expected only due to purely elastic deformation was calculated considering Eq. (2). The corresponding dependencies were represented by dotted lines in the upper right end of Fig. 7b. These lines have been plotted in an unrealistic extended elastic strain range to allow a better comparison of the curves. It can be seen that the experimental results obtained at the end of the loading path do reasonably follow the trend expected for a purely elastic deformation of the material which discards any ongoing transformation related processes in that region. On the other hand, the resistance values corresponding to 300 MPa at each temperature are, within experimental error, in good agreement with those obtained in the temperature-induced transformation under 300 MPa. This can be appreciated in Fig. 7a where the points $1^{\uparrow}$, $2^{\uparrow}$, $3^{\uparrow}$ fall close to the reference line included corresponding to cooling under 300 MPa constant applied stress. Due to the linear behavior exhibited by the reference *E.R.-T* curve in the temperature range below −75 °C no transformation activity is expected. This indicates that in all cases, similar degrees of transformation were stress-induced after loading to 300 MPa and thus similar volume fractions and variant orientations of the product phases were obtained.

On unloading from 300 MPa, the electrical resistance monotonically decreases to the values indicated at the right of Fig. 7b. The lower the temperature, the lower the value of resistance observed. This decrease of *E.R.* on unloading is similar for the three temperatures and is lower than 3.6% of the maximum *E.R.* values reached under 300 MPa. As was discussed when introducing Eq. (2), maximum variations in *E.R.* of about 0.2% may be attributed to elastic deformations during unloading. In all three experiments of Fig. 7, the temperature was below A_S and, therefore, it is expected that the volume fraction of martensite did not reduce on unloading. Then, the observed decrease in resistance must be a consequence of the reorientation of martensitic variants to accommodate internal stresses (a kind of rubber-like behavior). In principle, this also implies that the *E.R.* decreases despite of the possible introduction of new interfaces when passing from the stress-favored variant condition (300 MPa applied stress) to a more random distribution of twinned variants on unloading (6 MPa applied stress).

The evolution of the electrical resistance with deformation, Fig. 7b, may now be compared with the corresponding mechanical data, Fig. 7c. It turns out that at −100 °C two stages of nearly constant stress are observed. This mechanical behavior exhibiting two plateau type regions differ substantially from the one illustrated in Ref. [22]. In effect, in that case a single plateau, interpreted as corresponding to a process of reorientation of B19′ martensite variants, is observed. This difference is attributed to the R-phase which is absent in the case of the recrystallized microstructure used in Ref. [22] but clearly present in the UFG material studied here. For the curves in Fig. 7c corresponding to temperatures −125 °C and −150 °C it can be seen that both plateau-like regions are less differentiated when the testing temperature is decreased. Interestingly, the characteristic features exhibited by the mechanical data do not at all correspond to the electrical resistance evolution of Fig. 7b. The position of the resistance minima from Fig. 7b are indicated on the stress-strain curves of Fig. 7c and it can be seen that they are not associated with a singular point on the curve. Considering the resistive properties of the concomitant phases [13,14], the decrease in resistance in Fig. 7b detected at the beginning of loading might be attributed to the transformation from R-phase to B19′ martensite, finishing the process more or less at the same stress value. The subsequent increase of resistance would be mainly related to the reorientation of martensite variants that are already present at each test temperature. It can be noted that the stress values where the resistance minima occur, have a small temperature dependence with a slope of around $-0.2\ MPa/K$. This value is of the order of what can be deduced in the case of the reorientation of B19′ martensite variants grown in a recrystallized microstructure (around $-0.5\ MPa/K$ estimated from Fig. 6a in Ref. [22]). Notwithstanding, the present UFG wires do not present a well defined plateau attributable to reorientation, showing instead evidence of the process along an extended stress interval. As a consequence, the evolutions found in the experiments presented so far in Fig. 7 can be described in the following way:

(i) When reaching the test temperature, it can be supposed that the lower the temperature, the higher the amount of thermally-induced B19′ martensite will be. This phase is mostly randomly oriented.
(ii) On applying the load, the R-phase is transformed to B19′ martensite. As the latter structure is stress-induced, it is oriented according to the applied stress. Then, on reaching the minimum in the resistance curve of Fig. 7b, the whole sample will be mainly in the martensitic state. An evaluation of the data in Fig. 7b shows a resistance decrease of 5.2%, 5.8% and 3.4% (in order of decreasing temperatures) from the value at zero strain to that in the minimum. The main difference between the three cases is that for the lowest temperature there is a higher volume fraction of martensite that remains randomly oriented.
(iii) On further loading, the martensite reorients to fulfill the condition that a maximum elongation is obtained with a proper variant selection. On comparing the electrical resistance of the minimum in Fig. 7b to the value at the highest stress, increases of about 12%, 15% and 17% with decreasing temperature are found. This is in agreement with the state commented in the previous point, where the maximum amount of thermally induced reorientable martensite (instead of stress-induced B19′) is present at the lowest temperature.

From the present analysis, it can be inferred that three concomitant processes are responsible for the observed variation in *E.R.*: the transformation from R-phase to martensite (to lower *E.R.* values), the transformation from parent phase to martensite (to higher *E.R.* values), and the martensite reorientation (to higher *E.R.* values). All the previous consideration suggest that when loading the complex microstructure resulting from the temperature induced transformation different transformation and reorientation processes occur in varying degrees.

The final part of the loading experiments of Fig. 7 is presented next. As was noted above, the disordered variant configuration corresponding to the temperature-induced transformation condition is not fully recovered after completing a loading/unloading cycle. The evolution of electrical resistance of the latter microstructure was monitored during subsequent heating of these specimens, Fig. 7d. The resistance curve on heating of a load-free specimen (that was not subjected to a loading/unloading cycle)

was added to the diagram as a reference. It can be seen that the curves, although exhibiting some characteristics that are similar to those obtained on heating under constant applied loads, Fig. 3b, display a distinct different behavior. The dotted line added to the lower temperature points of curves 1, 2 and 3 exhibits a slope equal to the one observed at low temperature for the 300 MPa curve in Fig. 3b. The deviation of the resistance curves from this dotted line is an indication that, without an applied load and even at the lowest temperatures, retransformation events are taking place.

It can also be observed in Fig. 7d that the *E.R.* varies strongly in the temperature interval from −20 °C to around −3 °C. In the presence of a martensitic microstructural configuration of oriented variants, the resistance values decrease in this temperature range and upon reaching about −5 °C, the retransformation of martensite occurs in a sudden event in these unloaded specimens. On the contrary, *E.R.* monotonously increase in this same interval for the randomly oriented configuration. Therefore, a big loss of B19′ martensite stability associated with the abrupt change of *E.R.* appears to be independent of the previous thermomechanical story.

The distinct *E.R.* peak observed in the case of a random distribution of variants, located a few degrees higher, at around 0 °C, seems to shift vertically to higher *E.R.* values for the non-random cases (see Figs. 7d and 3b). It is found that the *E.R.* increases linearly with applied stress when analyzing the data corresponding to 6 MPa, 50 MPa and 100 MPa. Both results are in agreement with a dependence of the *E.R.* of the R-phase with the variant orientation, similar but of a lower magnitude than for B19′. This important finding indicates that the statement that the electrical resistance of the B2 phase is lower than that of B19′ martensite, which in turn is lower than that of the R-phase, all at the same temperature, is valid only for randomly oriented microstructures. When completely oriented, B19′ martensite exhibits the highest *E.R.* values. In all other cases, care has to be taken for the interpretation of the *E.R.* results. From the curves in Fig. 3a, this threshold stress level would be between 100 MPa and 150 MPa, i.e., at around the stress value where the localized transformation begins to manifest. This is a further confirmation that the process leading to the minimum *E.R.* in Fig. 7b is the stress-induced transformation from the R-phase to B19′ martensite.

4. Summary and conclusions

An ultra-fine grained Ti-50.9 at.% Ni shape memory alloy (commercial wire) was investigated by loading experiments under variable temperatures and stresses which resemble the loading condition in actuator applications. The occurring martensitic transformation events were studied by simultaneous resistance measurements. The current findings allow deriving the following main conclusions:

(1) In the case of temperature induced transformations under constant loads, a change from a homogeneous global transformation exhibiting limited but continuous deformation to a localized Lüders band type formation of B19′ martensite occurs upon cooling when the applied stress level exceeds a threshold value of around 130 MPa. Above this level, a sudden deformation of the ultra-fine grained material occurs after reaching a critical temperature which depends on the applied mechanical stress. Similar effects are observed upon heating.
(2) As a consequence of the deformation at constant temperature of complex microstructures resulting from previous temperature induced transformations, different further transformation and reorientation processes occur in varying degrees. Three concomitant processes are responsible for the observed variation in electrical resistance: (i) transformation from R-phase to martensite, (ii) transformation from parent phase to martensite, and (iii) martensite reorientation.
(3) Electrical resistance measurements proved that a simultaneous transformation involving both R-phase and B19′ martensites was always present in the extended range of temperatures and stresses investigated here, even though the strain evolutions do not always show two distinct yielding events during cooling or heating. The deformation of the wires on cooling can therefore be attributed to either the formation of the two martensitic phases or, in case of variable stress, to combinations of stress induced transformation plus reorientation reactions.
(4) Martensite reorientation processes seems to require stresses above 100 MPa in the present ultra-fine grained material. This value is still far lower than the minimum of 200 MPa observed in a recent study [22] on recrystallized NiTi with a grain size of 15 μm which shows a single-step transformation without R-phase.
(5) The electrical resistance of the B2 phase is lower than that of B19′ martensite, which in turn is lower than that of the R-phase, all at the same temperature in cases of randomly oriented microstructures. When completely oriented, B19′ martensite exhibits the highest electrical resistance values. In all other cases, care has to be taken for the interpretation of the electrical resistance results.
(6) Electrical resistance measurements constitute a simple and viable tool to assess the martensitic transformation process in ultra-fine grained NiTi which exhibits a high resistance against introduction of microstructural defects. Neither the elastic deformation of the involved phases nor the limited defect density even after repeated transformations have a significant effect on the obtained signals. Any obtained resistance variation can therefore directly be interpreted in terms of transformation events.

Acknowledgements

The authors acknowledge funding by the Deutsche Forschungsgemeinschaft DFG, Land Nordrhein-Westfalen and Ruhr University Bochum through the Collaborative Research Centre on Shape Memory Technology (SFB 459 Formgedächtnistechnik). AY and JLP acknowledge support from CNEA, CONICET, ANPCYT and U.N. Cuyo, Argentina.

References

[1] J. Van Humbeeck, Non-medical applications of shape memory alloys, Mater. Sci. Eng. A 273–275 (1999) 134–148.
[2] T. Duerig, A. Pelton, D. Stöckel, An overview of nitinol medical applications, Mater. Sci. Eng. A 273–275 (1999) 149–160.
[3] T. Saburi, Ti-Ni shape memory alloys, in: K. Otsuka, C.M. Wayman (Eds.), Shape Memory Materials, Cambridge University Press, 1998, pp. 49–96.
[4] Y. Kudoh, M. Tokonami, S. Miyazaki, K. Otsuka, Crystal structure of the martensite in Ti-49.2 at.%Ni alloy analyzed by the single crystal X-ray diffraction method, Acta Metall. 33 (1985) 2049–2056.
[5] E. Goo, R. Sinclair, The B2 to R transformation in Ti50Ni47Fe3 and Ti49.5Ni50.5 alloys, Acta Metall. 33 (1985) 1717–1723.
[6] A. Yawny, M. Sade, G. Eggeler, Pseudoelastic cycling of ultra-fine-grained NiTi shape-memory wires, Z. Metallkd. 96 (2005) 608–618.
[7] J.A. Shaw, S. Kyriakides, On the nucleation and propagation of phase transformation fronts in a NiTi alloy, Acta Mater. 45 (1997) 683–700.
[8] S. Gollerthan, M.L. Young, K. Neuking, U. Ramamurty, G. Eggeler, Direct physical evidence for the back-transformation of stress-induced martensite in the vicinity of cracks in pseudoelastic NiTi shape memory alloys, Acta Mater. 57 (2009) 5892–5897.
[9] L.C. Brinson, I. Schmidt, R. Lammering, Stress-induced transformation behavior of a polycrystalline NiTi shape memory alloy: micro and macro-mechanical investigations via in situ optical microscopy, J. Mech. Phys. Solids 52 (2004) 1549–1571.

[10] J. Olbricht, A. Yawny, J.L. Pelegrina, A. Dlouhy, G. Eggeler, On the stress induced formation of R-phase in ultra fine grained Ni-rich NiTi shape memory alloys, Metall. Mater. Trans. A 42 (2011) 2556–2574.
[11] S. Miyazaki, K. Otsuka, C.M. Wayman, The shape memory mechanism associated with the martensitic transformation in Ti-Ni alloys-I. Self-accommodation, Acta Metall. 37 (1989) 1873–1884.
[12] T. Waitz, The self-accommodated morphology of martensite in nanocrystalline NiTi shape memory alloys, Acta Mater. 53 (2005) 2273–2283.
[13] C.M. Hwang, M. Meichle, M.B. Salamon, C.M. Wayman, Transformation behaviour of a Ti50Ni47Fe3 alloy I. Premartensitic phenomena and the incommensurate phase, Philos. Mag. A 47 (1983) 9–30.
[14] C.M. Hwang, M. Meichle, M.B. Salamon, C.M. Wayman, Transformation behaviour of a Ti50Ni47Fe3 alloy II. Subsequent premartensitic behaviour and the commensurate phase, Philos. Mag. A 47 (1983) 31–62.
[15] K. Otsuka, X. Ren, Recent developments in the research of shape memory alloys, Intermetallics 7 (1999) 511–528.
[16] J. Khalil-Allafi, X. Ren, G. Eggeler, The mechanism of multistage martensitic transformations in aged Ni-rich NiTi shape memory alloys, Acta Mater. 50 (2002) 793–803.
[17] S. Miyazaki, T. Imai, K. Otsuka, Y. Suzuki, Lüders-like deformation observed in the transformation pseudoelasticity of a Ti-Ni alloy, Scripta Metall. 15 (1981) 853–856.
[18] J.A. Shaw, S. Kyriakides, Thermomechanical aspects of NiTi, J. Mech. Phys. Solids 43 (1995) 1243–1281.
[19] J.L. Pelegrina, A. Yawny, J. Olbricht, G. Eggeler, Transformation activity in ultrafine grained pseudoelastic NiTi wires during small amplitude loading/unloading experiments, J. Alloys Compd. 651 (2015) 655–665.
[20] J.M. Jani, M. Leary, A. Subic, M.A. Gibson, A review of shape memory alloy research, applications and opportunities, Mater. Des. 56 (2014) 1078–1113.
[21] A. Schaefer, M.F.-X. Wagner, J.L. Pelegrina, J. Olbricht, G. Eggeler, Localization events and microstructural evolution in ultra-fine grained NiTi shape memory alloys during thermo-mechanical loading, Adv. Eng. Mater. 12 (2010) 453–459.
[22] G. Laplanche, T. Birk, S. Schneider, J. Frenzel, G. Eggeler, Effect of temperature and texture on the reorientation of martensite variants in NiTi shape memory alloys, Acta Mater. 127 (2017) 143–152.
[23] J. Olbricht, Spannungsinduzierte Phasenumwandlungen und funktionelle Ermüdung in ultrafeinkörnigen NiTi-Formgedächtnislegierungen, vol. 17, Shaker Verlag, Aachen, Germany, 2008.
[24] J. Olbricht, Spannungsinduzierte Phasenumwandlungen und funktionelle Ermüdung in ultrafeinkörnigen NiTi-Formgedächtnislegierungen, Shaker Verlag, Aachen, Germany, 2008, pp. 25–26.
[25] G. Eggeler, E. Hornbogen, A. Yawny, A. Heckmann, M. Wagner, Structural and functional fatigue of NiTi shape memory alloys, Mater. Sci. Eng. A 378 (2004) 24–33.
[26] R. Vaidyanathan, M.A.M. Bourke, D.C. Dunand, Texture, strain, and phase-fraction measurements during mechanical cycling in superelastic NiTi, Metall. Mater. Trans. A 32 (2001) 777–786.
[27] J. Olbricht, Spannungsinduzierte Phasenumwandlungen und funktionelle Ermüdung in ultrafeinkörnigen NiTi-Formgedächtnislegierungen, Shaker Verlag, Aachen, Germany, 2008, pp. 115–117.
[28] J. Olbricht, A. Schäfer, M.F.-X. Wagner, G. Eggeler, Characterization of transformation localization during pseudoelastic cycling of NiTi, in: S. Miyazaki (Ed.), Proc. SMST 2007, ASM International, Materials Park, OH, 2007, pp. 47–54.